Application of Quasi Two Dimensional BEM Analysis in Ultrasonic Immersion Testing

Kwannate Tharmmapornphilas [1], Sohichi Hirose [2], Kazuyuki Nakahata [3]

1) Department of Mechanical and Environmental Informatics, Tokyo Institute of Technology
(2-21-1, O-okayama, Meguro-ku, Tokyo 152-8552, E-mail: kwannate@qnde.mei.titech.ac.jp)
2) Department of Mechanical and Environmental Informatics, Tokyo Institute of Technology
(2-21-1, O-okayama, Meguro-ku, Tokyo 152-8552, E-mail: shirose@cv.titech.ac.jp)
3) Department of Civil and Environmental Engineering, Ehime University
(3, Bunkyo, Matsuyama, Ehime 790-8577, E-mail: nakahata@dpc.ehime-u.ac.jp)

This paper presents a method to simulate the flaw signal, which is scattered by the side-drilled hole in the solid, in the ultrasonic immersion test. The equation of the linear time-shift invariant system, the multi-Gaussian beam model and the quasi boundary element method are applied to the numerical model. To compare with the experiment result, reflected wave by the flat surface of a specimen is used as a reference signal to determine the system efficiency factor. Simulation and experimental results are compared to verify the accuracy of the model.

Key Words : Multi-Gaussian beam model, Boundary element method, Ultrasonic wave, Flaw signal

1. Introduction

Ultrasonic non-destructive evaluation is widely conducted in steel industries for controlling quality of the products. For precise testing, ultrasonic immersion testing is used in automatic fashions to eliminate the need of couplants. However, ultrasonic detection of very small defects such as inclusions is very difficult with current ultrasonic testing. Therefore, the possibility to detect small flaws and the requirement of ultrasonic testing conditions should be studied in both experimental and theoretical works.

Wave propagation and reflection in ultrasonic immersion testing are complicated due to the presence of fluid-solid interface. However, using the multi-Gaussian beam model[1, 2], the wave field in solid can be efficiently simulated without complicated numerical procedure. Applying the linear time-shift invariant system[3], the ultrasonic measurement model with the same condition as the experiment could be obtained.

There are some researches on flaw detection using the combination of the linear time-shift invariant system and multi-Gaussian beam model[4, 5]. In those papers, the scattered wave from flaw is calculated in approximation way. Kitahara *et al.* and Nakahata *et al.* studied mechanisms of scattered waves using immersion testing by applying the multi-Gaussian beam model to the two dimensional BEM of flaws[6, 7]. However, in both papers, the experimental result is not shown.

The objectives of this study are, therefore, to develop the numerical model of the ultrasonic immersion testing and to verify the accuracy of the model by comparing the analytical results to the experimental results. The multi-Gaussian beam model is utilized for simulating the incidence wave field radiated from the immersion transducer. In order to observe the scattering of waves, the quasi two dimensional BEM[8] is applied to analyze the flaw model. Finally, the beam model is applied again to obtain the scattered wave spectrum in frequency domain. The waveform in time domain is determined by applying the inverse Fourier transform to the results in frequency domain. This simulated waveform is then compared to measured waveform from experiment to verify the accuracy of the model.

2. Multi-Gaussian Beam Model

The time harmonic pressure wave in fluid generated by the transducer is expressed using the multi-Gaussian beam model[1, 2] as

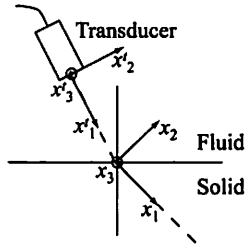

Fig. 1 Coordinate for multi-Gaussian beam model

$$p_{in}(\mathbf{x}',\omega)=\rho_f c_f v_0(\omega)\sum_{n=1}^{10}A_n\frac{\sqrt{\det\mathbf{G}^P(0)}}{\sqrt{\det\mathbf{G}^P(x_1')}}\exp\left\{ik_f x_1'\right\}\exp\left\{\frac{ik_f\left[\bar{x}'\right]^T\left[\mathbf{G}^P(x_1')\right]^{-1}\left[\bar{x}'\right]}{2}\right\} \quad (1)$$

where ρ_f is the density of fluid, c_f is the wave speed of fluid, k_f is the wave number in fluid, $v_0(\omega)$ is the velocity distribution on the surface of transducer, and

$$\mathbf{G}^P(0)=\begin{bmatrix}-\frac{ik_f d_0^2}{2B_n} & 0\\ 0 & -\frac{ik_f d_0^2}{2B_n}\end{bmatrix}, \quad (2)$$

$$\mathbf{G}^P(x_1')=\mathbf{G}^P(0)+x_1'\mathbf{I}, \quad (3)$$

$$\bar{x}'=\begin{pmatrix}x_2'\\ x_3'\end{pmatrix}. \quad (4)$$

The terms A_n and B_n are complex constants defined by Wen and Breazeale[9] as shown in Table 1 and d_0 is the radius of a transducer element. The references coordinate shows in Fig. 1.

When the Gaussian pressure wave transmits through the fluid-solid interface, the longitudinal and transverse waves are generated by the mode conversion. Using Snell's Law, the transmitted ray path for L and T waves in the solid can be defined. The displacement field in the solid due to the Gaussian pressure wave is given by

Table 1 Complex constants of Gaussian beam

n	A_n	B_n
1	11.428+0.95175i	4.0697+0.22726i
2	0.06002-0.08013i	1.1531-20.933i
3	-4.2743-8.5562i	4.4608+5.1268i
4	1.6576+2.7015i	4.3521+14.997i
5	-5.0418+3.2488i	4.5443+10.003i
6	1.1227-0.68854i	3.8478+20.078i
7	-1.0106-0.26955i	2.5280-10.310i
8	-2.5974+3.2202i	3.3197-4.8008i
9	-0.14840-0.31193i	1.9002-15.820i
10	-0.20850-0.23851i	2.6340+25.009i

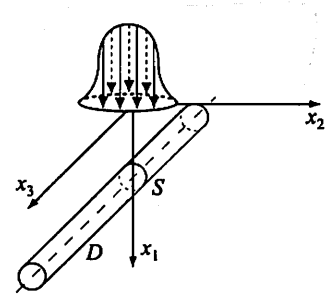

Fig. 2 The 3D-incident and 2D-scattered model

$$\boldsymbol{u}^{in}(\mathbf{x},\omega)=\sum_{\alpha=L,T}\frac{T^{\alpha;P}v_0(\omega)}{-i\omega}\boldsymbol{d}^{\alpha;P}\sum_{n=1}^{10}A_n\frac{\sqrt{\det\mathbf{G}^P(0)}}{\sqrt{\det\mathbf{G}^P(D_f)}}\frac{\sqrt{\det\mathbf{G}^P(0)}}{\sqrt{\det\mathbf{G}^P(x_1)}}\times\exp\left\{ik_f D_f+ik_\alpha x_1\right\}\exp\left\{\frac{ik_f\left[\bar{x}\right]^T\left[\mathbf{G}^\alpha(x_1)\right]^{-1}\left[\bar{x}\right]}{2}\right\} \quad (5)$$

$$\mathbf{G}^\alpha(x_1)=\mathbf{G}^P(D_f)+\frac{c_\alpha}{c_f}x_1\mathbf{I},\ \bar{x}=\begin{Bmatrix}x_2\\ x_3\end{Bmatrix} \quad (6)$$

where $T^{\alpha P}$ is the transmission coefficient of a plane wave propagated from fluid to solid, D_f is the distance between the interface and the transmitting transducer and $\boldsymbol{d}^{\alpha P}$ is the polarization direction.

Equation (5) is used as an incidence wave for quasi two-dimensional analysis shown in the next section.

3. Quasi Two-Dimensional Scattered Model

In a homogeneous elastic solid D, the displacement of the ultrasonic wave satisfies the equation of motion

$$C_{ijkl}u_{k,lj}(x,\omega)+\rho\omega^2u_i(x,\omega)=0, x\in D \quad (7)$$

where ρ is the density and ω is frequency. For an isotropic material, C_{ijkl} is given by

$$C_{ijkl}=\lambda\delta_{ij}\delta_{kl}+\mu\left(\delta_{ik}\delta_{jl}+\delta_{il}\delta_{jk}\right) \quad (8)$$

where λ and μ are the Lamé constants.

As shown in Fig. 2, the three-dimensional incident wave is applied to a scattering problem of infinite cylindrical hole in solid. The spatial Fourier transform with respect to x_3, where x_3 is taken in the longitudinal direction of the cylindrical hole, is defined by

$$\tilde{u}(X,\xi_3,\omega)=\int_{-\infty}^{\infty}u(X,\xi_3,\omega)\,e^{-i\xi_3 x_3}dx_3 \tag{9}$$

where $X=(x_1,x_2)$.

Applying the spatial Fourier transform to the equation of motion yields

$$C_{ijkl}\tilde{u}_{k,lj}(X,\xi_3,\omega)=-\rho\omega^2\tilde{u}_i(X,\xi_3,\omega) \tag{10}$$

Here, the original three-dimensional problem is transformed to a two dimensional problem. The boundary integral can be written as

$$\begin{aligned}\frac{1}{2}\left(\tilde{u}_k^M(X,\xi_3,\omega)-\tilde{u}_k^{in}(X,\xi_3,\omega)\right)&=\int_S\Big[U_{ik}^M(X,Y,\xi_3,\omega)\tilde{t}_i^M(Y,\xi_3,\omega)\\&-T_{ik}^M(X,Y,\xi_3,\omega)\tilde{u}_i^M(Y,\xi_3,\omega)\Big]dS_Y\\&-\int_S\Big[U_{ik}^M(X,Y,\xi_3,\omega)\tilde{t}_i^{in}(Y,\xi_3,\omega)\\&-T_{ik}^M(X,Y,\xi_3,\omega)\tilde{u}_i^{in}(Y,\xi_3,\omega)\Big]dS_Y\end{aligned} \tag{11}$$

where superscript M and 'in' refer to solid material and incident wave, respectively. By applying the Fourier transform to the three dimensional fundamental solution, the fundamental solution $U_{ik}(X,Y,\xi_3,\omega)$ can be obtained as follows[8]

$$\begin{aligned}&U_{ik}^M(X,Y,\xi_3,\omega)=\\&\frac{i}{4\mu}\left\{H_0^{(1)}(\tilde{k}_T R)\delta_{ik}+M_{ik}\left[H_0^{(1)}(\tilde{k}_T R)-H_0^{(1)}(\tilde{k}_L R)\right]\right\}\end{aligned} \tag{12}$$

where $H_0^{(1)}(\ )$ is the Hankel function of the zeroth order of the first kind, and

$$R=\left[\left(X_1-Y_1\right)^2+\left(X_2-Y_2\right)^2\right]^{1/2} \tag{13}$$

$$\tilde{k}_T=\left(k_T^2-\xi_3^2\right)^{1/2},\ \tilde{k}_L=\left(k_L^2-\xi_3^2\right)^{1/2} \tag{14}$$

where k_T and k_L are the transverse and longitudinal wave numbers defined by $k_T=\omega/c_T$ and $k_L=\omega/c_L$, respectively. In Eq. (12), M_{ik} is the following differential operator

$$\begin{aligned}M_{ik}=\frac{1}{k_T^2}\Bigg[&\delta_{\alpha k}\delta_{\beta i}\frac{\partial^2}{\partial X_\alpha\partial X_\beta}\\&-i\xi_3\left(\delta_{3k}\delta_{\alpha i}+\delta_{3i}\delta_{\alpha k}\right)\frac{\partial}{\partial X_\alpha}-\xi_3^2\delta_{3k}\delta_{3i}\Bigg]\end{aligned} \tag{15}$$

where, the summation with the Greek subscripts takes the values of 1 and 2 only. The traction kernel is defined by

$$T_{ik}^M(X,Y,\xi_3,\omega)=C_{k\beta jl}\frac{\partial U_{ij}(X,Y,\xi_3,\omega)}{\partial Y_l}n_\beta(Y) \tag{16}$$

Assuming the traction free boundary condition, the boundary integral equation in Eq. (11) is discretized and solved numerically for the boundary displacement on S. After determining the boundary displacement, the scattered displacement in solid is obtained as

$$\begin{aligned}u_i^{sc}(X,\xi_3,\omega)=&\int_S U_{ik}^M(X,Y,\xi_3,\omega)\tilde{t}_k^M(Y,\xi_3,\omega)dS_Y\\&-\int_S T_{ik}^M(X,Y,\xi_3,\omega)\tilde{u}_k^M(Y,\xi_3,\omega)dS_Y\end{aligned} \tag{17}$$

Introducing the far-field approximation, the scattered displacement in the solid can be reduced to

$$\tilde{u}_i^{sc:far}(X,\xi_3,\omega)=\sum_{\alpha=\mathrm{L,T}}\Omega_i^\alpha(\hat{X},\xi_3,\omega)\frac{\exp\left(i\left(\tilde{k}_\alpha|X|+\pi/4\right)\right)}{\sqrt{8\pi\tilde{k}_\alpha|X|}} \tag{18}$$

where

$$\begin{aligned}\Omega_i^\alpha(\hat{X},\xi_3,\omega)=&A_{ik}^\alpha(\hat{X},\xi_3,\omega)\int_S e^{-i\tilde{k}_\alpha(\hat{X}\cdot Y)}\tilde{t}_k^M(Y,\xi_3,\omega)dS_Y\\&-iB_{ijk}^\alpha(\hat{X},\xi_3,\omega)n_j(Y)\\&\int_S e^{-i\tilde{k}_\alpha(\hat{X}\cdot Y)}\tilde{u}_k^M(Y,\xi_3,\omega)dS_Y\end{aligned} \tag{19}$$

$$\begin{aligned}A_{ik}^T(\hat{X},\xi_3,\omega)=\delta_{ik}+\frac{1}{k_T^2}\Big[&-\hat{X}_i\hat{X}_k\tilde{k}_T^2\\&-\xi_3\tilde{k}_T\left(\delta_{3i}\hat{X}_k+\delta_{3k}\hat{X}_i\right)-\xi_3^2\delta_{3i}\delta_{3k}\Big]\end{aligned} \tag{20}$$

$$\begin{aligned}A_{ik}^L(\hat{X},\xi_3,\omega)=\frac{1}{k_T^2}\Big[&\hat{X}_i\hat{X}_k\tilde{k}_L^2+\\&\xi_3\tilde{k}_L\left(\delta_{3i}\hat{X}_k+\delta_{3k}\hat{X}_i\right)+\xi_3^2\delta_{3i}\delta_{3k}\Big]\end{aligned} \tag{21}$$

$$\begin{aligned}B_{ijk}^T(\hat{X},\xi_3,\omega)=&\frac{\lambda}{\mu}\delta_{jk}\Bigg\{-\tilde{k}_T\hat{X}_i-\xi_3\delta_{3i}+\\&\frac{1}{k_T^2}\left[\tilde{k}_T^3\hat{X}_i+\xi_3\tilde{k}_T^2\delta_{3i}+\xi_3^2\tilde{k}_T\hat{X}_i+\xi_3^3\delta_{3i}\right]\Bigg\}\\&-\tilde{k}_T\left(\delta_{ik}\hat{X}_j+\delta_{ij}\hat{X}_k\right)-\xi_3\delta_{3k}\delta_{ij}+\\&\frac{1}{k_T^2}\Big[2\hat{X}_i\hat{X}_j\hat{X}_k\tilde{k}_T^3+\xi_3\tilde{k}_T^2\\&\left(2\delta_{3i}\hat{X}_k\hat{X}_j+2\delta_{3k}\hat{X}_i\hat{X}_j\right)+2\xi_3^2\tilde{k}_T\delta_{3i}\delta_{3k}\hat{X}_j\Big]\end{aligned} \tag{22}$$

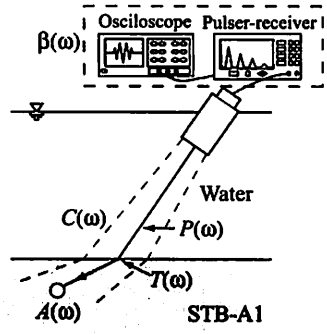

Fig. 3 Ultrasonic immersion testing system

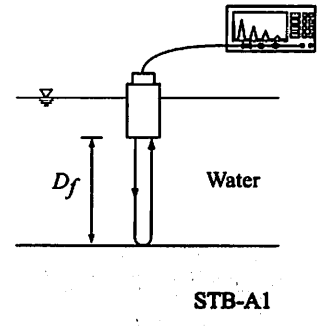

Fig. 4 Reference experimental setup

$$B_{ijk}^{\mathrm{L}}(\hat{X},\xi_3,\omega)=\frac{\lambda}{\mu}\delta_{jk}\left\{\frac{1}{k_{\mathrm{T}}^2}\left[-\tilde{k}_{\mathrm{L}}^3\hat{X}_i-\xi_3\tilde{k}_{\mathrm{L}}^2\delta_{3i}\right.\right.$$
$$\left.\left.-\xi_3^2\tilde{k}_{\mathrm{L}}\hat{X}_i-\xi_3^3\delta_{3i}\right]\right\}+\frac{1}{k_{\mathrm{T}}^2}\left[-2\hat{X}_i\hat{X}_j\hat{X}_k\tilde{k}_{\mathrm{L}}^3\right.$$
$$-\xi_3\tilde{k}_{\mathrm{L}}^2\left(2\delta_{3i}\hat{X}_k\hat{X}_j+2\delta_{3k}\hat{X}_i\hat{X}_j\right)$$
$$\left.-2\xi_3^2\tilde{k}_{\mathrm{L}}\delta_{3i}\delta_{3k}\hat{X}_j\right] \tag{23}$$

Applying the inverse Fourier transform to Eq. (18), the scattered displacement in three-dimensional space is obtained.

$$u_i^{sc:far}(\boldsymbol{x},\omega)=\sum_{\alpha=\mathrm{L,T}}\frac{1}{2\pi}\int_{-\infty}^{\infty}\Omega_i^{\alpha}(\hat{X},\xi_3,\omega)$$
$$\frac{\exp\left(i\left(\tilde{k}_{\alpha}|X|+\pi/4\right)\right)}{\sqrt{8\pi\tilde{k}_{\alpha}|X|}}\exp\left(ix_3\xi_3\right)d\xi_3$$
$$=\sum_{\alpha=\mathrm{L,T}}u_i^{sc:far:\alpha}(\boldsymbol{x},\omega) \tag{24}$$

4. Linear Time-Shift Invariant (LTI) System

Figure 3 illustrates the immersion ultrasonic testing model based on the linear time-shift invariant system. The voltage output V from a flaw, shown in oscilloscope, can be written according to the LTI system[3] as

$$V(\omega)=\beta(\omega)M(\omega)P_{in}(\omega)C_{in}(\omega)T_{in}(\omega)$$
$$A(\omega)T_{sc}(\omega)C_{sc}(\omega)P_{sc}(\omega) \tag{25}$$

where $\beta(\omega)$ is the system efficiency factor, $M(\omega)$ is the attenuation in fluid and solid, $P(\omega)$ is the wave propagation, $C(\omega)$ is the beam pattern of transducer, $T(\omega)$ is a transmission coefficient at fluid-solid interface, and $A(\omega)$ is the scattered wave from flaw. In this paper, the attenuation term $M(\omega)$ is neglected.

4.1. Incident wave

In Eq. (25), the term of $P_{in}(\omega)C_{in}(\omega)T_{in}(\omega)$ is considered as the incidence wave in the solid just before hitting the hole, which is expressed by Eq. (5). The components of the incident α (α = L, T) wave can then be written as

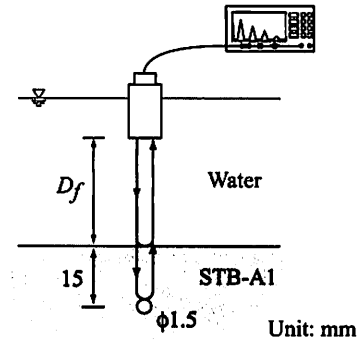

Fig.5 Experimental setup

$$P_{in}^{\alpha}(\omega)=\exp\left\{ik_f D_f+ik_{\alpha}x_1\right\} \tag{26}$$

$$C_{in}^{\alpha}(\omega)=\sum_{n=1}^{10}v_0(\omega)A_n\frac{\sqrt{\det\mathbf{G}^P(0)}}{\sqrt{\det\mathbf{G}^P(D_f)}}\frac{\sqrt{\det\mathbf{G}^P(0)}}{\sqrt{\det\mathbf{G}^P(x_1)}}$$
$$\exp\left\{\frac{ik_f\left[\bar{\mathbf{x}}\right]^T\left[\mathbf{G}^{\alpha}(x_1)\right]^{-1}\left[\bar{\mathbf{x}}\right]}{2}\right\} \tag{27}$$

$$T_{in}^{\alpha}(\omega)=-\frac{T^{\alpha;P}}{i\omega}d^{\alpha;P} \tag{28}$$

Hence, we have

$$u^{in}(\boldsymbol{x},\omega)=P_{in}(\omega)C_{in}(\omega)T_{in}(\omega)$$
$$=\sum_{\alpha=L,T}P_{in}^{\alpha}(\omega)C_{in}^{\alpha}(\omega)T_{in}^{\alpha}(\omega) \tag{29}$$

4.2. Scattering from flaw

u^{in} is used as an input to the quasi two dimensional scattering model. After the numerical analysis, the scattered wave result from quasi two dimensional BEM is obtained. However, when an original three dimensional problem is considered, the far-field scattered displacement is written as

$$u_i^{sc:far3D}(\boldsymbol{x},\omega)=\sum_{\beta=\mathrm{L,T}}\Omega_{3D}^{\beta}(\hat{\boldsymbol{x}},\omega)\frac{\exp\left(ik_{\beta}|\boldsymbol{x}|\right)}{|\boldsymbol{x}|} \tag{30}$$

Comparing Eq. (24) to Eq. (30), Ω_{3D}^{β} is expressed in terms of the solution of quasi two dimensional BEM analysis $u^{sc;far;\beta}$ as follows

$$\Omega_{3D}^{\beta}(\hat{x},\omega)=\frac{|x|}{\exp\left(ik_{\beta}|x|\right)}u_i^{sc:far:\beta}(x,\omega) \tag{31}$$

If the incidence wave were a plane wave with unit amplitude, then Ω_{3D}^{β} had corresponding to $A^{\beta}(\omega)$, where $A^{\beta}(\omega)$ is the component of $A(\omega)$ for the scattered β wave.

In this study, however, the incident wave is given by the multi-Gaussian beam model as shown in Eq. (29). Thus the radiation pattern Ω_{3D}^{β} given by Eq. (31) can be written by

$$\begin{aligned}\Omega_{3D}^{\beta}(\hat{x},\omega)&=\frac{|x|}{\exp\left(ik_{\beta}|x|\right)}u_i^{sc:far:\beta}(x,\omega)\\&=P_{in}(\omega)C_{in}(\omega)T_{in}(\omega)A^{\beta}(\omega)\end{aligned} \tag{32}$$

4.3. Back propagation

Finally, $P_{sc}(\omega)C_{sc}(\omega)T_{sc}(\omega)$ in Eq. (25) is the back propagation. The components of the back propagation $\beta(\beta=\mathrm{L,T})$ wave can be written as

$$P_{sc}^{\beta}(\omega)=\exp\left\{ik_f D_f+ik_{\beta}x_1\right\} \tag{33}$$

$$C_{sc}^{\beta}(\omega)=\frac{2}{-ik_{\alpha}d_0^2}\sum_{n=1}^{10}v_0(\omega)A_n\frac{\sqrt{\det\mathbf{G}^P(0)}}{\sqrt{\det\mathbf{G}^P(D_f)}}\frac{\sqrt{\det\mathbf{G}^P(0)}}{\sqrt{\det\mathbf{G}^P(x_1)}}\exp\left\{\frac{ik_f[\bar{\mathbf{x}}]^T\left[\mathbf{G}^{\beta}(x_1)\right]^{-1}[\bar{\mathbf{x}}]}{2}\right\} \tag{34}$$

$$T_{in}^{\beta}(\omega)=\rho_s c_{\alpha}i\omega T^{\beta;P}\boldsymbol{d}^{\beta;P} \tag{35}$$

Here, the average of scattered wave over the transducer surface is included. The equation for the simulation voltage output $V(\omega)$ of the scattered wave from side-drilled hole can be written as

$$\begin{aligned}V(\omega)&=\Omega_{3D}(\omega)P_{sc}(\omega)C_{sc}(\omega)T_{sc}(\omega)\\&=\sum_{\alpha=L,T}\Omega_{3D}^{\beta}(\omega)P_{sc}^{\beta}(\omega)C_{sc}^{\beta}(\omega)T_{sc}^{\beta}(\omega)\end{aligned} \tag{36}$$

4.4. Reference Model and System Efficiency Factor

Figure 4 shows the reference experimental setup. The JIS-standard calibration block A1 (STB-A1) is used. The waveform of the echo reflected from the surface of STB-A1 is acquired as a reference signal. Applying Fourier transform, the wave spectrum V_R of the reference experiment is obtained.

For this reference experimental setup, the LTI system equation can be written as

$$V_R(\omega)=\beta(\omega)P_{in}(\omega)C_{in}(\omega)R\ C_{sc}(\omega)P_{sc}(\omega) \tag{37}$$

where R is the reflection coefficient of a plane wave at the fluid-solid interface calculated analytically. Considering at a center line of probe, the simulation of reflected wave on the surface of STB-A1 is

$$\begin{aligned}&P_{in}(\omega)C_{in}(\omega)R\ C_{sc}(\omega)P_{sc}(\omega)\\&=\exp\left(2ik_f D_f\right)\left[\sum_{n=1}^{10}A_n\frac{\sqrt{\det G^P(0)}}{\sqrt{\det G^P(D_f)}}\right]^2 R\frac{2D_f}{-ik_f d_0^2}\\&=O_R(\omega)\end{aligned} \tag{38}$$

Here, the term $\frac{2D_f}{-ik_f d_0^2}$ of Eq. (38) is the correction factor corresponding to the average of scattered wave over the received transducer surface. The exponential term of $C(\omega)$ is ignored. The system efficiency factor can be calculated by

$$\beta(\omega)=\frac{V_R(\omega)}{O_R(\omega)} \tag{39}$$

To compare the simulation result to the experiment result, Eq. (36) is multiplied by the system efficiency factor $\beta(\omega)$.

5. Comparison between Experiment and Simulation

The transducer used in this experiment is the Panametrics V306, which has the center frequency of 2.25 MHz, and the element diameter is 13 mm. The specimen used in this study is a standard calibration block A1 (STB-A1), with the side-drilled hole of 1.5 mm-diameter at 15 mm-depth from the top surface, as shown in Fig. 5. Both ends of side-drilled hole are attached with the water resistant adhesive tapes to protect the hole from water. The material properties of STB-A1 are c_L = 5900 m/s, c_T = 3246 m/s and density = 7900 kg/m^3. The wave velocity of water is 1480 m/s and density is 1000 kg/m^3.

Figure 6 shows the reference waveform, which is reflected from the front surface of STB-A1, and its spectrum. The simulation result of flaw echo scattered wave is shown in Fig. 7(a). The result of the experiment is shown in Fig. 7(b). Here, the echo from the front surface of specimen is also shown. It should be noted that the flaw echo obtained from the simulation is in a very good agreement with that obtained from the real experiment in terms of waveform and amplitude.

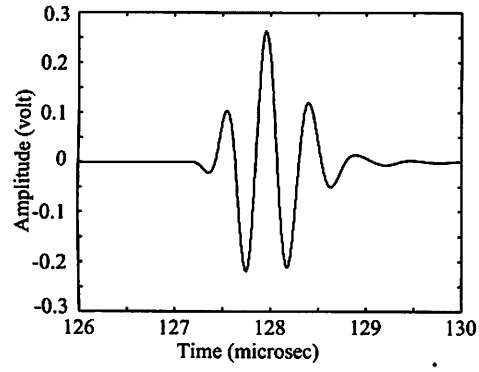

(a) Waveform

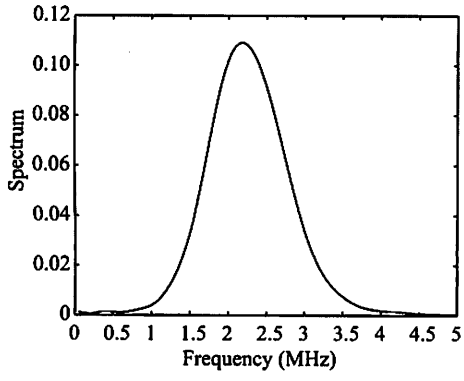

(b) Wave spectrum

Fig. 6 The experimental reference signal reflected from the front surface of specimen (D_f= 94 mm)

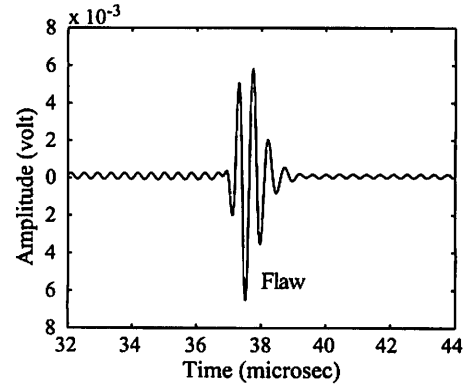

(a) Simulation

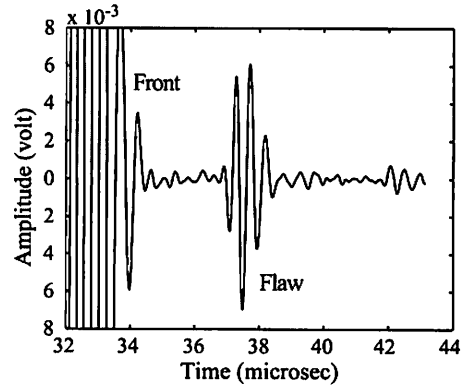

(b) Experiment

Fig. 7 Flaw signal from side-drilled hole (D_f= 23 mm)

6. Summary

In this paper, the numerical model of the flaw signal in the immersion test is developed based on the multi-Gaussian beam model and BEM. The main advantage of this model is to predict the flaw signal wave, which will appear on oscilloscope.

The simulation and experiment of ultrasonic detection of the side-drilled hole in STB-A1 were conducted in order to verify efficiency and accuracy of the proposed model. The result of this model shows a very good accuracy and reliability.

In the further work, the proposed model will be used to study the possibility of the ultrasonic detection of small defects.

References

(1) Schmerr, L. W., A multigaussian ultrasonic beam model for high performance simulation on a personal computer, *Materials Evaluation* 58(7), pp.882-888, 2000.

(2) Rudolph, M., *Ultrasonic beam models in anisotropic media*, Ph.D thesis, Iowa State University, 1999.

(3) Thompson, R. B. and Gray, T. A., Model relating ultrasonic scattering measurement through liquid-solid interfaces to unbounded medium scattering amplitude, *J. Acoust. Soc. Am.* 74(4), pp.1279-1290, 1983

(4) Kim, H. J., Song, S. J. and Schmerr, L. W., Modeling ultrasonic pulse-echo signal from a flat-bottom hole in immersion testing using a multi-gaussian beam, *Journal of Nondestructive Evaluation* 23(1), pp.11-19, 2004.

(5) Kim, H. J., Park, J. S., Song, S. J. and Schmerr, L. W., Modeling angle beam ultrasonic testing using multi-gaussian beam, *Journal of Nondestructive Evaluation* 23(3), pp.81-93, 2004.

(6) Kitahara, M., Nakahata, K. and Ichino, T., Application of BEM for the visualization of scattered wave fields from flaws, *Review of Progress in Quantitative Nondestructive Evaluation* 23, pp.43-49, 2004.

(7) Nakahata, K. and Hirose, S., A modeling of ultrasonic testing and simulation of scattered wave from flaws, *Journal of Applied Mechanics JSCE* 7, pp.271-278, 2004.

(8) Li, Z. L., Achenbach, J. D., Komshy, I. and Lee, Y. C., Reflection and transmission of obliquely incident surface waves by an edge of a quarter space: theory and experiment, *J. Appl. Mech. ASME* 59, pp.349-355, 1992.

(9) Wen, J. J. and Breazeale, M. A., A diffraction beam field expressed for description of sound diffraction, *J. Acoust. Soc. Am.* 83(5), pp.1752-1756, 1988.